Acta Materialia 144 (2018) 411–418

Contents lists available at ScienceDirect

Acta Materialia

journal homepage: www.elsevier.com/locate/actamat

Full length article

Relaxation and saturation of electrostriction in 10 mol% Gd-doped ceria ceramics

Nimrod Yavo [a], Ori Yeheskel [b], Ellen Wachtel [a], David Ehre [a], Anatoly I. Frenkel [c], Igor Lubomirsky [a, *]

[a] Department of Materials and Interfaces, Weizmann Institute of Science, Israel
[b] Department of Materials, Nuclear Research Center Negev, Beer-Sheva, Israel
[c] Department of Materials Science and Chemical Engineering, Stony Brook University, NY, United States

ARTICLE INFO

Article history:
Received 20 July 2017
Received in revised form
24 October 2017
Accepted 25 October 2017
Available online 30 October 2017

Keywords:
Gd-doped ceria
Electrostriction
Grain boundaries
Impedance spectroscopy

ABSTRACT

10 mol% Gd-doped ceria (10GDC) ceramics, with grain size in the single micron range, display electrostrictive behavior under ambient conditions of temperature and pressure. In weak, quasi-static electric fields, i.e. <1 kV/cm, frequency <1 Hz, the longitudinal strain is measured to be proportional to the square of the applied electric field, albeit with the corresponding electrostrictive strain coefficient (M_{33}) displaying large variability between samples: $-(2\text{-}20)\cdot10^{-17}$ (m/V)^2. Nevertheless, $|M_{33}|$ of all samples exceeds the values expected on the basis of the classical (Newnham) electrostriction scaling law by up to two orders of magnitude. A systematic study reveals the functional dependence of M_{33} on frequency: above 10 Hz, $|M_{33}|$ decreases to $\approx10^{-18}$ (m/V)^2, which may be characterized as non-Debye relaxation with non-ideality factor 0.35–1.13. For frequencies $\leq$1.5 Hz, increasing the field strength beyond 1 kV/cm results in an exponential decrease in $|M_{33}|$: the longitudinal strain saturates at 1-4 ppm. Dielectric impedance spectra suggest that partitioning of the applied voltage between grain boundaries and grain cores may be a factor contributing both to the large variability in the electrostriction parameters, and to the strong dependence on electric field amplitude. The frequency dependence may have two sources: the slow electric field-driven reorganization of the Ce-containing active complexes in the electrostrictive medium as well as the influence of the grain boundaries. 10GDC ceramics may therefore be added to the list of non-classical electrostrictors which includes reduced and Gd-doped ceria thin films and (Nb,Y)-doped bismuth oxide ceramics.

1. Introduction

Electromechanically active materials (electrostrictors and piezoelectrics) are essential components of a large variety of technologies ranging from focusing devices in cellular phone cameras to sonar. Electrostriction is an electromechanical response, proportional to the square of the applied electric field amplitude, which may be displayed by all dielectrics, independent of crystal symmetry. For a uniaxial electric field applied parallel to the z-axis,E_3, the longitudinal (z-directed) strain is described by $u_3 = M_{33}\cdot E_3^2$, where M_{33} (m^2/V^2) is the corresponding electrostriction strain coefficient (M_{33} is Voigt notation for M_{ijkl}, a fourth-rank, symmetric tensor). More than two decades ago, Robert Newnham [1] reported the results of an extensive study of *polarization* electrostriction coefficients, Q, (e.g., for z − directed strain: $u_3 = Q_{33}\cdot P_3^2$, where $Q_{33} = M_{33}/(\varepsilon\cdot\varepsilon_0)^2$ and $P_3 = \varepsilon\varepsilon_0 E_3$ is the longitudinal polarization;ε is the material dielectric constant and ε_0 is the vacuum permittivity). He noted that for diverse electroactive materials, a linear relationship is observed on a log-log plot of the hydrostatic polarization electrostriction coefficient $|Q_h|$ *vs.* the ratio of the material elastic compliance to the dielectric constant. Indeed, polymers, glasses, linear dielectrics and relaxors, all characterized by either large elastic compliance or large dielectric constants, obey this scaling law. In 2012, our group reported that thin films of 20 mol% Gd-doped ceria (20GDC) exhibit an in-plane electrostrictive strain coefficient of 6.47×10^{-18} m^2/V^2 at 0.1Hz, exceeding by at least two orders of magnitude what would be expected on the basis of the low values of material compliance and dielectric constant [2]. Continuing this work, we examined ceramic pellets of cubic $Bi_7Nb_{2-x}Y_xO_{15.5-x}$(x = 0.4–1.6) and found that they also

* Corresponding author.
E-mail address: igor.lubomirsky@outlook.com (I. Lubomirsky).

https://doi.org/10.1016/j.actamat.2017.10.056
1359-6454/

demonstrate non-classical electrostriction with $|M_{33}| = 0.3–1.3 \times 10^{-17}$ m^2/V^2, the value increasing with vacancy concentration [3]. Similar to GDC, the $Bi_7Nb_{2-x}Y_xO_{15.5-x}$ fluorite crystal lattice contains oxygen vacancy-generated point defects, although many more, and is markedly anelastic [3–5]. Recently, Hadad et al. ([6]) have reported the modulating effects of different film preparation protocols and electrode metals on the magnitude of the electrostrictive response of 20GDC thin films.

X-ray absorption techniques- EXAFS (extended X-ray absorption fine structure), XANES (X-ray absorption near-edge structure), HERFD (high energy resolution X-ray fluorescence detection) - have been successfully applied to identify the electromechanically active species of Gd-doped ceria and to characterize the resulting lattice distortions [7,8]. Analysis of *in situ* EXAFS measurements of 10GDC thin films, with electric field modulation, indicated that the average field-free strain of the active Ce-O bonds can reach -4.7% but only 3.3% of such ion pairs in the lattice are affected, while the majority are "spectators". These data can more than account for the ≈0.01–0.05% macroscopic strain observed in the 10GDC films [2,9]. HERFD, combined with modeling, was used to characterize the three-dimensional geometry of the electromechanically active units [10] with and without an external electric field. The best fit model of the field-free lattice of 10GDC films is based on randomly distributed changes in length of the Ce-O bonds in the vicinity of oxygen vacancies, produced by one or both types of lattice defects: (i) displacement of oxygen ions parallel to the fluorite crystal (111) direction, (ii) shift of Ce ions along the (010) direction. In contrast to classical electrostrictors and piezoelectrics, the induced strain is therefore not uniform over the whole sample, but is rather generated locally and averaged.

The aim of the current study was to determine if the non-classical electrostrictive behavior of GDC is limited to thin film geometry, or is also observed for ceramic pellets of similar chemistry. The choice of 10GDC was based on the extensive structural and mechanical data already available for this composition. Although the pellets are clearly electrostrictive, the fact that as the frequency of the applied electric field increases, longitudinal strain is weakened, points to the slow kinetics of reorganization of the active complexes in the lattice. The longitudinal strain saturation, observed below 1.5Hz as a function of electric field amplitude and not reported in the previous studies of GDC films, may be attributable to the blocking activity of the grain boundaries.

2. Experimental

2.1. Preparation of $Ce_{0.9}Gd_{0.1}O_{1.95}$ ceramic pellets

The preparation of $Ce_{0.9}Gd_{0.1}O_{1.95}$(10GDC) ceramic pellets followed the protocol described earlier in Ref. [11]. The green body was sintered in air in a two-step procedure [12], with the maximum temperatures in the first and second stage, T_1 and T_2 respectively, adjusted to control the grain size (Table 1). Subsequent cooling was accomplished at 5 °C/min, a process which is sufficiently slow to ensure depth-independent sample stoichiometry as controlled by the level of aliovalent doping. We produced a set of ceramic pellets 8-11 mm diameter and 1–2.8 mm thickness. The density of the pellets was determined by the Archimedes method and by geometric measurements. To support the data obtained by the Archimedes method and to verify the absence of microcracks, the ultrasound pulse echo technique [11,13] was also used. Scanning electron microscopy (SEM, Supra 55 FEG Zeiss HRSEM) was used to determine grain size *via* the linear intercept method (i.e., counting how many grains fit into a straight line of known length drawn over an SEM image [14]), counting more than 100 grains and then the average observed intercept value was multiplied by a factor of 1.56 [14]. Composition was verified with energy dispersive X-ray spectroscopy (EDS, Bruker XFlash 6-60). Phase determination and lattice parameter calculations were accomplished with X-ray diffraction (XRD, Rigaku TTRAXIII, variable slits; analysis with Jade (MDI)). Prior to measurement of electrostriction, the pellets were mirror polished, finishing with SiC P4000 (5 μm) grade polishing paper, and then annealed for 3 h at 500 °C under O_2 (heating/cooling rate 2.5 °C/min). The obligatory polishing with a water-based slurry necessitated subsequent annealing in O_2 for 3 h at 500 °C in order to eliminate damage to the surface layer, which can occur to a depth of up to a few microns. This includes changes in the concentration of oxygen vacancies, adsorption of water molecules and stress-related defects. The annealing process removes residual traces of water [15], which otherwise could result in surface proton conductivity, while the effective diffusion length of oxygen during the annealing process is more than sufficient to restore surface layer stoichiometry [16].

2.2. Electrostrictive strain measurements

Electrostrictive strain was measured in an air-conditioned laboratory, in which the temperature was controlled within the range 24 ± 2 °C. The relative humidity in the room varied from 20% to 55% depending on the external weather conditions and was recorded prior to each experiment. We did not observe correlation of our experimental results with recorded variations in relative humidity. The instrumentation was constructed on a proximity sensor-based system of the capacitance type (Lion) with lock-in detection, as described previously [3]. Longitudinal electrostrictive strain (parallel to the applied electric field) is calculated as a ratio between the absolute displacement of a pushrod pressed onto the sample surface by a spring as measured by the proximity sensor and the original thickness of the ceramic pellets. The sensor sensitivity is 1.9 mV/nm displacement. The lock-in amplifier provides RMS voltage at the second harmonic of the applied electric field (cf. the experimental section in Ref. [3]). The diameter of the sensor is 3 mm and prior to measurement, the sensor and the pushrod top surface are aligned to better than 2°. The sample is polished to ensure that upper and lower surfaces are parallel to within accuracy 1:100. Therefore, very precise lateral alignment of the sample/electrode stack is not required (cf. Fig. 3a in Ref. [3]). The system has an absolute sensitivity of ≈0.05 nm (at 0.1 Hz), which corresponds to strain measurement of (0.05 nm/1 mm) = 0.05 ppm for a 1 mm thick sample. Sensitivity increases with increasing frequency to 500Hz, while the applied voltage can be varied within the range 50–2000 V. The system was calibrated with commercial samples of PZT (Shenzhen Yujie Electronics Co. Ltd. China; our measurement d_{33} = 450 ± 20 p.m./V); PMN-PT (TRS Technologies; our measurement M_{33}= (3.5 ± 0.5) × 10^{-16} m^2/V^2) and a 100-cut quartz single crystal (our measurement d_{33} = 2.3 ± 0.2 pm/V). We have verified the stability of the system specifically for 10GDC pellets by conducting measurements alternately with insertion and removal of the sample. Single sample $|M_{33}|$ measurement reproducibility was high (±5%; e.g., Figure SI1) and the consistency of results is therefore primarily determined by the uniformity of sample characteristics and electrical contacts. During measurement of the electromechanical response, the 10GDC pellets were sandwiched between two metal plates. The top electrode was 3 mm thick aluminum with lateral dimensions 31 mm × 25 mm, while the bottom electrode was brass. That part of the bottom electrode on which the ceramic was placed is disk-shaped with diameter 12 mm and thickness, 2 mm. That part of the electrode which is in contact with the sample holder, is 2.5 mm thick and 25 mm in diameter. The pellets were glued to the bottom plate with silver paint under a force of ≈10 N. The top plate was pressed to the sample during the

Table 1
Characteristics of the 10GDC ceramic pellets prepared using the two-step sintering procedure (T1,T2) in air as described in the Experimental section; additional treatment; grain size and pellet thickness (*th*). The density of all samples was above 97% (closed porosity).

Sample ID	Sintering procedure, °C		Additional treatment	Grain size, μm	*th*, mm
	T_1	T_2			
P09-01	1450	1150	3 h at 500 °C in O_2	0.79 ± 0.26	2.83
P09-02	1300	1100	"	0.63 ± 0.05	2.33
P09-04	1300	1100	"	0.47 ± 0.14	2.66
P09-06*	1450	1150	"	0.57 ± 0.03	1.47
P09-10	1550	1150	"	1.50 ± 0.11	1.59
P05-02	1500	1250	"	1.22 ± 0.08	1.60
P05-03	1500	1250	"	1.25 ± 0.16	1.68
P06-03	1450	1100	"	0.95 ± 0.08	2.48
P06-06	1400	1100	6 h at 1500 °C in air; 3 h at 500 °C in O_2	3.58 ± 0.3	2.67
P09-01 HT1	1450	1150	20 h at 1350 °C in air; 3 h at 500 °C in O_2	1.36 ± 0.57	2.83
P09-01 HT2	1450	1150	50 h at1450 °C in air; 3 h at 500 °C in O_2	5.6 ± 2.34	2.83
P09-01 HT2p	1450	1150	50 h at 1450 °C in air; polishing; 3 h at 500 °C in O_2	5.6 ± 2.34	1.40
P09-01 HT2pp	1450	1150	50 h 1450 °C in air; polishing; 3 h at 500 °C in O_2	5.6 ± 2.34	0.86

T_2 dwell time was 6 min.

measurement with a force of 1 N.

2.3. Impedance spectroscopy

Room temperature impedance spectroscopy measurements were conducted with a Novocontrol Alfa dielectric analyzer in high voltage mode on pellets, which were located inside or outside of the electrostriction measurement instrument. In the latter case, upper and lower electrical contacts were made with silver paint. Applied voltages were: 10 VAC, 1 MHz–1 mHz; 0-135 VDC. Measured impedance values fall within the 1% accuracy range of the impedance analyzer [17].

3. Results

As reported recently [11], the dual temperature sintering protocol used in this study consistently produces ceria ceramics with specific density greater than 96%. Such dense pellets, containing topologically closed intergrain pores, are relatively robust, permit accurate structural characterization, and, in addition, do not permit pore-to-pore protonic conductivity which, at lower ceramic densities, may be present under ambient conditions, deriving from adsorbed water molecules [15]. X-ray diffraction of the 10GDC pellets revealed a fluorite lattice with lattice parameter $a = 0.54181 \pm 4 \times 10^{-5}$ nm at 25 °C (Fig. 1a: sample P06-06). The average grain size of the 10GDC pellets was in the range 0.47–1.50 μm, depending in particular on sintering temperature T_1 (Table 1, Fig. 1b: sample P09-01). Further high temperature treatment produced limited additional grain growth, as shown in Fig. 1c and d for the same sample. Gd content, as determined by EDS, did not differ between samples by more than 0.5 mol%.

3.1. Longitudinal electrostrictive strain: saturation and relaxation

All 10GDC ceramic pellets tested exhibited electromechanical response at the second harmonic of the applied electric field (E) for the complete range of field amplitudes and frequencies (f) applied. The samples contract in the direction of the field, which agrees with the previously reported negative longitudinal electrostrictive strain in thin GDC films [9] and in (Y,Nb)-stabilized bismuth oxide ceramics [3]. At electric fields below 1 kV/cm, the longitudinal strain (u) is proportional to E^2 (Fig. 2a and b): samples P06-03 and P06-06), which, together with the proximity monitor response only at the second harmonic, clearly identifies the effect as electrostriction. Below 10 Hz, the longitudinal strain displays saturation with increasing electric field amplitude (Fig. 2a and b), while the small field electrostrictive strain coefficient (M_{33}) decreases markedly with frequency (Fig. 2c): samples P06-03 and P06-06 (Fig. 3). The

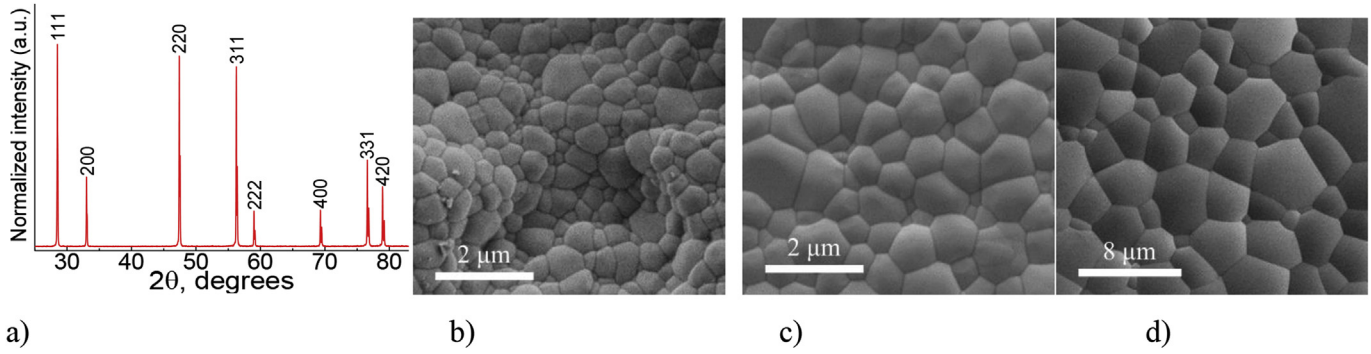

Fig. 1. a) XRD pattern of the 10GDC pellet P06-06 (prior to heating under O_2) measured in Bragg-Brentano mode with variable slit widths. The (hkl) indices correspond to diffraction peaks of the fluorite cubic lattice (ICSD #2879). b) SEM image of the as-sintered pellet P09-01. The average grain size is 0.79 μm. c) The same sample after grain growth at 1350 °C for 20 h. The average grain size is 1.36 μm. d) The same sample after grain growth at 1450 °C for 50 h. The average grain size is 5.6 μm.

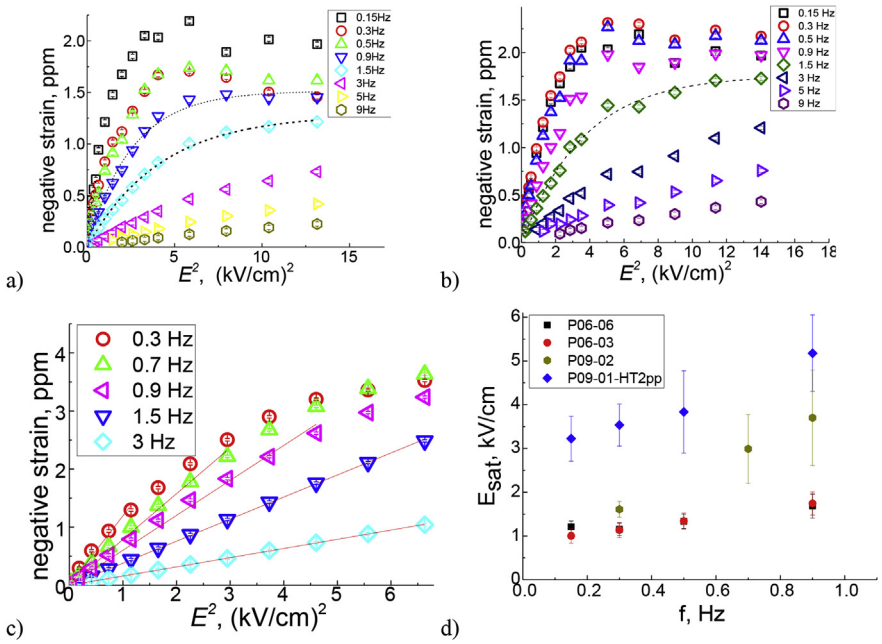

Fig. 2. Longitudinal negative strain as a function of the square of the applied electric field at frequencies 0.15 - 9Hz, showing strain saturation behavior for (a) sample P06-03 and (b) sample P06-06. Dashed lines represent the results of fitting to Equation (1); (c) low field, linear fits for pellet P09-02. (d) Frequency dependence of E_{sat} (Equation (2) for samples P06-06, P06-03, P09-02, P09-01-HT2pp).

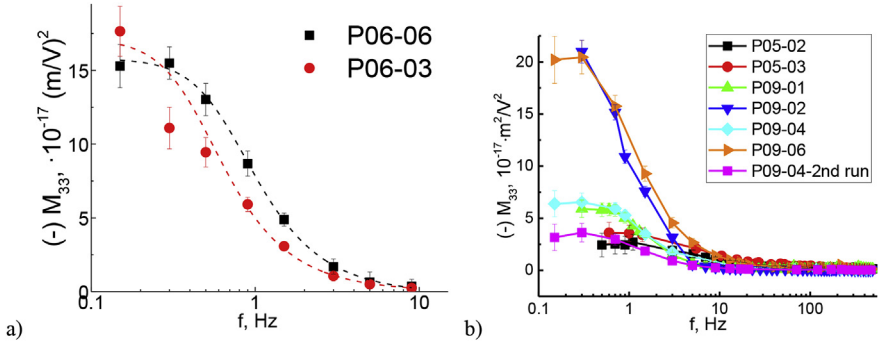

Fig. 3. a) Relaxation of M_{33} for samples P06-06 and P06-03 at applied field <4 kV/cm for frequencies <10Hz. Dashed lines represent the results of fitting to Equation (2); (b) Frequency dependent relaxation of M_{33} up to 500Hz for P09 and P05 sample pellets (Table 2) at applied field < 10 kV/cm.

field-dependent strain saturation can be described by Equation (1):

$$u\left(E^2\right) = M_{33}\cdot E_{sat}^2\cdot\left[1-\exp\left(-E^2\Big/E_{sat}^2\right)\right], \quad (1)$$

where M_{33} is the electrostrictive strain coefficient at f < 1.5 Hz, E < 2.5 kV/cm; E_{sat} denotes the saturation field, above which the relationship between the strain and E^2 is no longer linear. E_{sat} is frequency dependent and takes values of 1–5 kV/cm up to 1.5 Hz (Fig. 2d). $u_{sat} = M_{33}\cdot E_{sat}^2$ is the saturation strain which is found to be only 1-4 ppm [2]. The relaxation of the electrostriction strain coefficients as a function of frequency ($M_{33}(f)$), can be fit by the (non-ideal Debye) expression:

$$M_{33}(f) = \frac{M_{33}^{o}}{\sqrt{(\tau\cdot f)^{2+\alpha}+1}} + M_{33}^{\infty}, \quad (2)$$

where M_{33}° and M_{33}^{∞} are the low and high frequency values of, $M_{33}(f)$ respectively. Relaxation times in the range τ = 0.27–2.17 s and non-ideality factors α = -0.35–1.13 are found for the samples measured without thinning or grain growth-promoting thermal treatment. The unusually large values of the non-ideality parameter indicate that the active complexes responsible for the electrostrictive behavior have a broad distribution of relaxation times. The fitting parameters for Equation (2) for these samples are summarized in Table 2.

The classical (Newnham) scaling law for electrostrictors takes the form of a log-log plot of the hydrostatic electrostriction polarization coefficient $|Q_h|$ *vs* $S/\varepsilon\varepsilon_o$, where S is the material elastic compliance, ε is the dielectric constant, ε_o is the vacuum permittivity [1], and for isotropic or cubic materials, $Q_h = Q_{11} + 2Q_{12} = Q_{11}\cdot(1-2\cdot\nu)$, where Q_{11} and Q_{12} are the longitudinal and transverse electrostriction polarization coefficients and ν is Poisson's ratio. The low frequency, room temperature dielectric constant of 10GDC is $\varepsilon \approx 28$; the elastic compliance is $S \approx 4.6\cdot 10^{-12}\ Pa^{-1}$ and the Poisson's ratio is 0.315 (the latter two values are from Ref. [11]). Therefore, $|Q_h|$ for 10GDC ceramics at low frequencies is estimated [3] to be 150-1500 m^4/C^2, which is larger than observed for both (Nb,Y)-doped cubic bismuth oxide ceramics and GDC thin films and is more than two orders of

Table 2
Summary of the best fit values for the parameters in Equation (2) for 10GDC pellets prepared as described in the Experimental section and Table 1: the low frequency longitudinal electrostrictive strain coefficient M_{33}^{0}; Debye relaxation time τ, non-ideality factor α and high frequency limiting values M_{33}^{∞}. The samples contract along the direction of the field. Therefore, $M_{33}^{o}<0$.

Sample ID	$(-)M_{33}^{o}$, $10^{-17}m^2/V^2$	M_{33}^{∞},$10^{-18}m^2/V^2$	τ, s	α
P09-01	5.9 ± 0.1	−1.51 ± 0.1	0.88 ± 0.02	1.13 ± 0.11
P09-02-	16.8 ± 0.3	0.01 ± 0.20	2.17 ± 0.08	0.64 ± 0.08
P09-04	6.52 ± 0.08	0.83 ± 0.29	0.90 ± 0.03	0.80 ± 0.12
P09-04[a]	3.35 ± 0.08	0.45 ± 0.29	0.91 ± 0.06	0.70 ± 0.22
P09-06	20.8 ± 0.3	−1.84 ± 0.54	1.23 ± 0.03	0.35 ± 0.06
P09-10	21.7 ± 1.1	−1.23 ± 0.16	1.69 ± 0.1	0.88 ± 0.07
P05-02	2.38 ± 0.08	−1.71 ± 0.21	0.27 ± 0.02	0.22 ± 0.18
P05-03	3.65 ± 0.07	−1.18 ± 0.16	0.32 ± 0.02	−0.35 ± 0.07
P06-03	18.6 ± 0.3	−0.99 ± 0.45	3.43 ± 0.11	0.55 ± 0.07
P06-06	14.7 ± 0.3	1.74 ± 0.86	1.94 ± 0.09	0.92 ± 0.18
P09-01-HT1	10.4 ± 0.2	2.2 ± 0.7	0.65 ± 0.04	0.75 ± 0.20
P09-01, HT2	9.2 ± 0.4	1.06 ± 0.73	2.36 ± 0.19	0.42 ± 0.18
P09-01, HT2p[b]	14.5 ± 0.3	2.16 ± 0.96	1.26 ± 0.06	0.17 ± 0.11
P09-01, HTpp[b]	14.7 ± 0.2	2.3 ± 1.2	1.34 ± 0.07	0.65 ± 0.19

[a] The P09-04 sample was removed from the proximity measurement instrument, replaced and re-measured. These results are unique with respect to non-reproducibility.
[b] Measured four times alternately with inserting and removing the sample from the proximity measurement instrument.

magnitude greater than the value expected [1] for a material characterized by $S/\varepsilon_o\varepsilon = 0.022$. At low electric field amplitudes, but above 10Hz, $|M_{33}|$ decreases to $\approx 1 \times 10^{-18}$ m^2/V^2(±20% for all samples), which corresponds to $|Q_h| = 6.5$ m^4/C^2, which is still approximately one order of magnitude higher than the prediction of the classical model [1].

3.2. Dependence of the electrostrictive strain on grain size and sample thickness

In an attempt to explain the large sample-to-sample variability in M_{33}^{o}, α and τ (Table 2), we altered the grain size and thickness of a single pellet, P09-01 (Table 1; Table 2). In particular, we have considered the possibility that differences in stoichiometry between grain interiors and grain boundaries, specifically oxygen vacancy concentration differences, may play a role in this variability. We have systematically subjected a sample to two stages of grain growth, thereby stepwise reducing the volume fraction of grain boundaries in the pellet: first from 0.79 μm to 1.36 μm (P09-01HT1) and then from 1.36 μm to 5.6 μm (P09-01HT2). Nevertheless, no systematic changes in the measured electrostriction parameters were detected. The thickness of the sample was then reduced in two stages by polishing: from 2.83 mm to 1.4 mm (P09-01HT2p) and then to 0.86 mm (P09-01HT2pp). The first polishing produced an increase in M_{33}^{o}, while further reduction in thickness did not have any significant effect. The values of α and τ which characterize strain relaxation did not change in a consistent way in response to these treatments (Table 2).

3.3. Impedance spectroscopy (IS)

Since limited changes in 10GDC pellet structural parameters did not appear to determine electromechanical behavior, electrical impedance was investigated. The Nyquist plots for all pellet samples, with impedance measured at room temperature, comprised two depressed semi-circular arcs (e.g., Fig. 1a, pellet P09-04): the low frequency arc has a much larger radius than that appearing at high frequencies. IS measurements, both inside and outside the electrostriction apparatus (with electrode configurations as described in the Experimental section), displayed very similar features for the high frequency arc (Figure SI2). The high Z_{re} intersection of the smaller of the two arcs occurs at frequency <1 Hz, while that of the larger arc occurs close to 1 mHz. To assist in assigning the arcs to the ceramic grain interior, grain boundaries or electrical contacts, IS spectra were measured with varying constant voltage bias U_{DC} (Fig. 4a). The radius of the larger arc is observed to decrease under increasing bias (Fig. 4b), thereby eliminating the possibility that this low frequency arc is due to the grain interior [18–20]. In fact, the radius of the larger arc is also sensitive to removing and remaking of the electrical contacts (data not shown), so contact resistance appears to be the most likely source. The radius of the high frequency arc was only marginally influenced by U_{DC}.

Interpretation of the origin of the smaller of the two arcs on the basis of the room temperature impedance data is not conclusive. However, performing IS measurements on pellet P09-04 at moderately elevated temperatures (80-150 °C) outside the electrostriction apparatus, provided some clarification. As expected, raising the temperature produced an overall reduction in sample impedance (≈1000-fold). The radius of the smaller arc in the Nyquist plots contracted with increasing temperature from ~ 2GOhm at room temperature to 1 MOhm at 106 °C. In addition, at the higher temperatures, a third arc became apparent (Fig. 5a and b). On this basis, we concluded that only at elevated temperature could the grain boundary impedance be separated from that of the grain interior. However, the current–voltage characteristics of grain boundaries (I_{gb} –U_{gb}) in ion conducting ceramics are often complex [21,22]. Recently, grain boundaries in acceptor-doped ceria have been shown, both experimentally and theoretically [18–20], to exhibit power-law (n) dependence of I_{gb} vs U_{gb}. For $U_{gb} < V_{th}$, (where $V_{th} = kT/q$), n ≈ 1 (i.e. ohmic behavior), whereas when U_{gb} is significantly greater than V_{th}, n > 1 (i.e., superohmic).

Fig. 6 demonstrates that between 95 and 150 °C and with $V_{dc} \geq 50V$, the grain boundaries in 10GDC pellets studied here display superohmic behavior (n~1.5) even for $U_{gb} < V_{th}$. It is not possible to identify similar behavior at room temperature, since the semicircle, representing grain boundary impedance on those Nyquist plots cannot be properly distinguished and its radius measured. Nevertheless, Fig. 6 suggests the possibility that even at room temperature, mixed ionic-electronic conduction is present in the grain boundaries, thereby promoting charge accumulation [18–20].

4. Discussion

4.1. Unifying principles of non-classical electrostriction in ionic conductors

While most common, efficient electrostrictors have been characterized by large values of dielectric constant and/or elastic

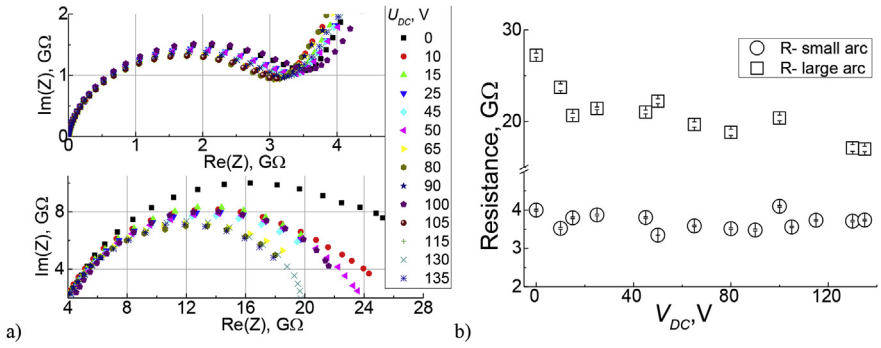

Fig. 4. a) Room temperature Nyquist plots for pellet P09-04 under 0-135 V DC bias, 10 V AC, frequency range 1 MHz-1mHz, measured using Ag paste electrodes. The upper plot is an enlargement of the frequency range in which electrostriction was measured (1 MHz-150 mHz), the bottom plot is an enlargement of the frequency range 150 mHz-1mHz. b) Resistance values determined from the two impedance semicircles on the room temperature Nyquist plot of pellet P09-04 as a function of applied DC bias V_{DC}. Resistance values were calculated by fitting the Nyquist plots to a circular arc. Resistance is then calculated from twice the arc radius.

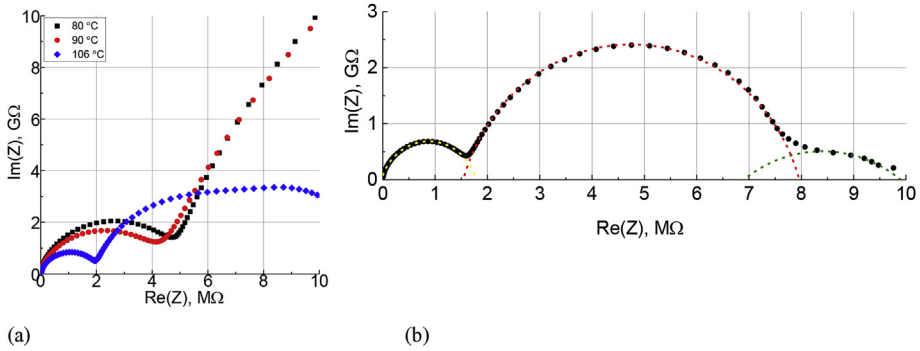

Fig. 5. a) Nyquist plot of pellet P09-04 at elevated temperatures (80-106 °C) measured under 10 V AC and 0 V DC (b) Nyquist plot of pellet P09-04 measured at 106 °C under 10 V AC and 50 V DC bias. Dashed lines represent the semi-circle fitting result for grain interior (yellow), grain boundaries (red) and contacts (green). (For interpretation of the references to colour in this figure legend, the reader is referred to the web version of this article.)

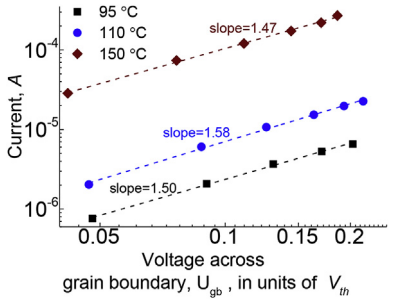

Fig. 6. I-V curves for grain boundaries in the 10GDC ceramic (sample P09-04) as estimated from IS measurements with $10V_{ac}$ and 50-135 U_{DC} at 95 °C, 110 °C and 150 °C (*viz.* Fig. 5). The current $I = U_{DC}/R_{total}$, where R_{total} is the sum of the resistances of the grain interiors, grain boundaries and electrode interface. At and above T = 95 °C and U_{DC} = 50V, the electrode interface resistance is not significant. $U_{gb} = (U_{DC} \cdot R_{gb}/R_{total})/N_{gb}$, where N_{gb} is estimated as: the pellet thickness divided by the average grain diameter. For the graph abscissa, U_{gb} is given in units of V_{th} = kT/q.

compliance [23], a new class of electrostrictive materials has recently been identified for which both the dielectric constant and elastic compliance are low [3]. Included are substrate-supported thin films of reduced ceria and of Gd-doped ceria, up to 33 mol% Gd [2,9]; and (Nb,Y)-doped bismuth oxide ceramics [3]. These materials all display high ionic conductivity at elevated temperature resulting from the oxygen vacancies formed in response to cation reduction or aliovalent doping; cubic fluorite lattice symmetry; and anelastic behavior, detected by nanoindentation measurement of room temperature creep. Electrostrictive coefficients have been measured under ambient conditions [2,3,9] and have been found to be significantly larger than predicted by the Newnham scaling law [1]. Supported by XAS findings, the unusually large electromechanical activity has been attributed to the electric field-generated response of a small population of strongly anharmonic chemical bonds (cation-O) with lattice positions in the vicinity of the oxygen vacancies.

4.2. Material properties and measurement conditions of non-classical electrostrictors

4.2.1. Comparison of electromechanical activity: GDC films, GDC and (Nb,Y)-doped Bi_2O_3 ceramics

A range of material properties and measurement conditions characterize previous studies of non-classical electrostrictors. An electric field applied to 300-500 nm thick, (111) textured, reduced ceria and Gd-doped ceria films, supported on cantilevers, was observed to produce in-plane stress [2] and *via* the known elastic properties of the films [4], the in-plane strain was calculated. For electric fields up to 60 kV/cm and with frequency 0.1Hz, the in-plane electrostrictive strain coefficient (M_{31}) was determined to vary from (2-16) $\times$ $10^{-18}(m/V)^2$ depending on film composition. Somewhat lower values have been reported more recently by Hadad et al. [6] for 2 μm thick, (111) textured, 20GDC films supported on cantilevers, with electric fields up to 400 kV/cm. The largest value of the in-plane strain coefficient was $M_{31} = 9 \times 10^{-19}$ $(m/V)^2$ measured at 66 Hz. A marked reduction in M_{31} was noted at frequencies above 100 Hz; the choice of electrode metal was also observed to modulate the electrostrictive response. In the case of

(Nb,Y) − doped cubic bismuth oxide ceramic pellets (10 mm diameter, 0.9–1.1 mm thick, 15-40 μm grain size), negative longitudinal strain was observed for voltage <1500 V, and frequency between 20 Hz and 1.2 kHz. In this frequency range, the strain was linear with the square of the applied field up to 11 kV/cm. The measured values of M_{33} = -0.47 to -1.2 × 10^{-17}(m/V)^2, depended on the cation doping levels. In thin films of GDC, the electrostrictive strain can reach hundreds of ppm and even with fields as high as 60 kV/cm, there is no indication of saturation [9].

In the current work, we have returned to the study of the electromechanical behavior of GDC, but here 10GDC in the form of a ceramic pellet, rather than a thin film, with 0.47–5.6 μm grain size and 0.86–2.83 mm thickness. Our measurements, for the first time, systematically monitor the influence of both the field amplitude and frequency on the nature and magnitude of the electromechanical response of this class of electrostrictors. We have observed both frequency relaxation and strain saturation. Due to the lack of systematic characterization of the effects of frequency in the earlier works, we cannot definitively determine to what extent the present results are consistent with previous measurements [2,3,9]. Concerning relaxation, the electromechanical response of GDC thin films was not measured in the relevant frequency range (150 mHz-20 Hz) by either Korobko et al. [2] or Hadad et al. [6] With respect to strain saturation: GDC thin films on cantilevers display no obvious strain saturation at least until 60 kV/cm, 0.1Hz [2] or 400 kV/cm, 66 Hz [6]. Bismuth oxide ceramics do not demonstrate obvious strain saturation until at least 11 kV/cm at frequency >20Hz. However, we note that the present work shows obvious strain saturation only for frequencies below 1.5Hz with onset at about 1 kV/cm.

4.2.2. Open questions regarding non-classical electrostrictors

Since strain saturation in 10GDC ceramics is a function of electric field frequency, that may be true for the other non-classical electrostrictive materials as well, but the earlier reports do not provide sufficiently detailed information to either verify or eliminate the possibility of strain saturation. We must also ask whether sample morphology, i.e. films on cantilevers vs. ceramic pellets, could be expected to influence strain saturation behavior. Certainly, systematic measurements of both relaxation and strain saturation should be performed on the other three systems. Until that is done, we cannot say if the behavior we observe for 10GDC ceramics is representative of the entire class of non-classical electrostrictors, or it is due to particular material properties, such as blocking grain boundaries. The fact that the single high frequency semicircle on the room temperature Nyquist plot can be resolved into two semicircles at T ≥ 95 °C,U_{DC}≥50V, suggests that, under the conditions of our electromechanical measurements, i.e. room temperature without DC bias, there is significant voltage drop on both the grain boundaries and grain interiors [24–27]. In addition, the superohmic behavior of grain boundary resistivity at elevated temperatures, even for DC bias < V_{th}, provides evidence for charging due to electron trapping.

Since charging is a time-dependent process, it would be expected to be more significant at lower frequencies, leading to saturation of the electromechanical response at lower field amplitudes when the frequency is lowered. Grain boundary charging may also produce some type of non-uniform distribution of voltage [24–26,28–31] throughout the sample volume, e.g. as discrete layers of high field intensity, resulting in the observation of larger displacement than in the case of a homogeneous voltage distribution, as well as the possibility of increased sample-to-sample variability. In such a situation, the electrostriction strain coefficient, as measured by the proximity sensor at low frequencies (<10 Hz), could be an overestimate.

5. Conclusions

In summary, we have demonstrated that dense, ceramic pellets of 10 mol % Gd doped-ceria (10GDC) display non-classical electrostriction with marked dependence on both (i) frequency and (ii) amplitude of the applied electric field. (i) The room temperature, longitudinal electrostrictive strain coefficient M_{33} exhibits non-ideal Debye frequency dependence with reduction of up to two orders of magnitude from ~0.3Hz to ~10Hz. A model for the origin of the electromechanical activity of GDC, derived from X-ray absorption measurements on thin films, suggests that relaxation at relatively low frequencies may be a general material property for non-classical electrostrictors. It derives, at least in part, from the slow kinetics of field-induced reorganization of the small population of active complexes, comprising a Ce ion with octahedral coordination of 7 oxygen ions + one oxygen vacancy. (ii) Strain saturation has not been reported for the previously identified, non-classical electrostrictors, i.e., GDC thin films or (Nd,Y) doped bismuth oxide ceramics. In 10GDC ceramics, the longitudinal, electrostrictive strain does saturate in applied fields larger than ~1 kV/cm, (<1.5Hz). The dependence of the impedance spectra on DC bias and sample temperature measured for these samples is interpreted as pointing to charge trapping or voltage re-distribution at the grain boundaries and electrical contacts as likely being responsible. Obviously, more work is required in order to resolve these complexities, to fully characterize this new class of electromechanically active materials and to put them to practical use.

Acknowledgements

IL and AIF acknowledge the NSF-BSF program grant 2015679. AIF acknowledges support by NSF Grant number DMR-1701747. This work was supported by the Israeli Ministry of Science and Technology grant 3-12944. This research is made possible in part by the historic generosity of the Harold Perlman Family.

Appendix A. Supplementary data

Supplementary data related to this article can be found at https://doi.org/10.1016/j.actamat.2017.10.056.

References

[1] R.E. Newnham, V. Sundar, R. Yimnirun, J. Su, Q.M. Zhang, Electrostriction: nonlinear electromechanical coupling in solid dielectrics, J. Phys. Chem. B 101 (1997) 10141–10150.
[2] R. Korobko, A. Patlolla, A. Kossoy, E. Wachtel, H.L. Tuller, A.I. Frenkel, I. Lubomirsky, Giant electrostriction in Gd-doped ceria, Adv. Mater. 24 (2012) 5857–5861.
[3] N. Yavo, A.D. Smith, O. Yeheskel, S.R. Cohen, R. Korobko, E. Wachtel, P.R. Slater, I. Lubomirsky, Large nonclassical electrostriction in (Y, Nb)-Stabilized δ-Bi_2O_3, Adv. Func. Mat. 26 (2016) 1138–1142.
[4] R. Korobko, S.K. Kim, S. Kim, S.R. Cohen, E. Wachtel, I. Lubomirsky, The role of point defects in the mechanical behavior of doped ceria probed by nano-indentation, Adv. Func. Mat. 23 (2013) 6076–6081.
[5] A.S. Nowick, B.S. Berry, Anelastic Relaxation in Crystalline Solids, Academic Press, 1972.
[6] M. Hadad, H. Ashraf, G. Mohanty, C. Sandu, P. Muralt, Key-features in processing and microstructure for achieving giant electrostriction in gadolinium doped ceria thin films, Acta Mat. 118 (2016) 1–7.
[7] A. Kossoy, Q. Wang, R. Korobko, V. Grover, Y. Feldman, E. Wachtel, A.K. Tyagi, A.I. Frenkel, I. Lubomirsky, Evolution of the local structure at the phase transition in CeO_2-Gd_2O_3 solid solutions, Phys. Rev. B 87 (2013) 1–4.
[8] A. Kossoy, A.I. Frenkel, Q. Wang, E. Wachtel, I. Lubomirsky, Local structure and strain-induced distortion in $Ce_{0.8}Gd_{0.2}O_{1.9}$, Adv. Mat. 22 (2010) 1659–1662.
[9] R. Korobko, A. Lerner, Y.Y. Li, E. Wachtel, A.I. Frenkel, I. Lubomirsky, In-situ extended X-ray absorption fine structure study of electrostriction in Gd doped ceria, Appl. Phys. Lett. 106 (2015). Artn 042904.
[10] Y.Y. Li, O. Kraynis, J. Kas, T.C. Weng, D. Sokaras, R. Zacharowicz, I. Lubomirsky, A.I. Frenkel, Geometry of electromechanically active structures in Gadolinium - doped Cerium oxides, AIP Adv. 6 (2016). Artn 055320.

[11] N. Yavo, D. Noiman, E. Wachtel, S. Kim, Y. Feldman, I. Lubomirsky, O. Yeheskel, Elastic moduli of pure and gadolinium doped ceria revisited: sound velocity measurements, Scr. Mat. 123 (2016) 86–89.
[12] I.W. Chen, X.H. Wang, Sintering dense nanocrystalline ceramics without final-stage grain growth, Nature 404 (2000) 168–171.
[13] O. Yeheskel, O. Tevet, Elastic moduli of transparent yttria, J. Am. Ceram. Soc. 82 (1999) 136–144.
[14] M.I. Mendelson, Average grain size in polycrystalline ceramics, J. Am. Ceram. Soc. 52 (1969) 443–446.
[15] G. Lazovski, E. Wachtel, Y. Tsur, I. Lubomirsky, Using ellipsometry with lock-in detection to measure activation energy of ion diffusion in ionic and mixed conductors, Sol. State Ionics 264 (2014) 7–16.
[16] P.S. Manning, J.D. Sirman, J.A. Kilner, Oxygen self-diffusion and surface exchange studies of oxide electrolytes having the fluorite structure, Sol. State Ionics 93 (1996) 125–132.
[17] Alfa Novocontrol Impedance Analyzer Specification, page 7, https://www.novocontrol.de/pdf_s/alphspec.pdf. Last accessed on 23rd. Oct. 2017.
[18] S.K. Kim, S. Khodorov, I. Lubomirsky, S. Kim, A linear diffusion model for ion current across blocking grain boundaries in oxygen-ion and proton conductors, Phys. Chem. Chem. Phys. 16 (2014) 14961–14968.
[19] S. Kim, S.K. Kim, S. Khodorov, J. Maier, I. Lubomirsky, On determining the height of the potential barrier at grain boundaries in ion-conducting oxides, Phys. Chem. Chem. Phys. 18 (2016) 3023–3031.
[20] S.K. Kim, S. Khodorov, C.T. Chen, S. Kim, I. Lubomirsky, How to interpret current-voltage relationships of blocking grain boundaries in oxygen ionic conductors, Phys. Chem. Chem. Phys. 15 (2013) 8716–8721.
[21] R. Bouchet, P. Knauth, T. Stefanik, H.L. Tuller, Impedance and Mott-Schottky analysis of a $Pr_{0.15}Ce_{0.85}O_{2-x}$ solid solution, Solid State Ionics 756 (2003) 169–174.
[22] P.F. Yan, T. Mori, A. Suzuki, Y.Y. Wu, G.J. Auchterlonie, J. Zou, J. Drennan, Grain boundary's conductivity in heavily yttrium doped ceria, Sol. State Ionics 222 (2012) 31–37.
[23] TRS technologies, Electrostrictors Brochure; http://www.trstechnologies.com/Materials/Electrostrictive-Ceramics; Last accessed 23 Oct. 2017.
[24] A. Jasper, J.A. Kilner, D.W. McComb, TEM and impedance spectroscopy of doped ceria electrolytes, Sol. State Ionics 179 (2008) 904–908.
[25] H. Hojo, T. Mizoguchi, H. Ohta, S.D. Findlay, N. Shibata, T. Yamamoto, Y. Ikuhara, Atomic structure of a CeO2 grain boundary: the role of oxygen vacancies, Nano Lett. 10 (2010) 4668–4672.
[26] T. Zacherle, A. Schriever, R.A. De Souza, M. Martin, Ab initio analysis of the defect structure of ceria, Phys. Rev. B 87 (2013).
[27] B.W. Sheldon, V.B. Shenoy, Space charge induced surface stresses: implications in ceria and other ionic solids, Phys. Rev. Lett. 106 (2011).
[28] B.O.H. Grope, T. Zacherle, M. Nakayama, M. Martin, Oxygen ion conductivity of doped ceria: a Kinetic Monte Carlo study, Sol. State Ionics 225 (2012) 476–483.
[29] M. Nakayama, M. Martin, First-principles study on defect chemistry and migration of oxide ions in ceria doped with rare-earth cations, Phys. Chem. Chem. Phys. 11 (2009) 3241–3249.
[30] J. Hinterberg, T. Zacherle, R.A. De Souza, Activation volume tensor for oxygen-vacancy migration in strained CeO2 electrolytes, Phys. Rev. Lett. 110 (2013).
[31] Y.U. Shi, A.H. Bork, S. Schweiger, J.L.M. Rupp, The effect of mechanical twisting on oxygen ionic transport in solid-state energy conversion membranes, Nat. Mat. 14 (2015) 721–727.